D0 Note 6305-CONF

Search for the standard model Higgs boson in tau lepton pair final states

The DØ Collaboration
(Dated: March 5, 2012)

We present a search for the standard model Higgs boson in final states with an electron or muon and a hadronically decaying tau lepton in association with zero, one, or two or more jets using up to 7.3 fb^{-1} of Tevatron collider data collected with the D0 detector. The analysis is sensitive to Higgs boson production via gluon gluon fusion, associated vector boson production, and vector boson fusion, and to Higgs boson decays to tau lepton pairs or W boson pairs. Observed (expected) limits are set on the ratio of 95% C.L. upper limits on the cross section times branching ratio to those predicted by the Standard Model of 14.3 (21.8) at a Higgs mass of 115 GeV and 7.7 (6.8) at 165 GeV.

Preliminary Results for 2012 Winter Conferences

I. INTRODUCTION

The standard model (SM) of particle physics postulates a complex Higgs doublet field as the source of electroweak symmetry breaking, giving rise to non-zero masses of the vector bosons and fundamental fermions. The mass of the SM spin-zero Higgs boson, H, that survives after the symmetry breaking is not predicted, but is constrained by direct searches at the LEP [1], Tevatron [2] and LHC [3] colliders, and by precision measurements of W and Z boson and top quark properties [4] to be in the range 115 – 127 GeV at the 95% C.L. Over the mass range $115 \leq m_H \leq 150$ the Higgs boson decay branching fractions vary considerably, with $H \to b\bar{b}$ ($H \to \tau^+\tau^-$) being the dominant (subdominant) decays for a Higgs mass $m_H \leq 135$ GeV and $H \to W^+W^-$ ($H \to ZZ$) becoming important for $m_H > 135$ GeV. Previous analyses by the D0 [5] and CDF [6] Collaborations have mainly focused on the decay modes $H \to b\bar{b}$ in the low mass region and $H \to WW$ with both W bosons decaying to an electron or muon in the high mass region.

A previous D0 publication [7] reported a Higgs boson search in the tau lepton pair plus two jets final state, with one tau decaying to a muon and the other to hadrons, using 1.0 fb^{-1} of data. In this Letter, we report the results of three searches involving tau pair production that extend those results by adding more data, increasing the trigger efficiency, adding new search channels, and considering additional signal contributions. The final states used are: (*i*) $\mu\tau$ plus zero or one jet (denoted $\mu\tau$01), (*ii*) $\mu\tau$ plus two or more jets ($\mu\tau$2+), and (*iii*) $e\tau$ plus two or more jets ($e\tau$2+). The $\mu\tau$01, $\mu\tau$2+, and $e\tau$2+ analyses use respectively 7.3, 6.2 and 4.3 fb^{-1} of data collected with the D0 detector [8]. Here and in the following, "τ_h" represents a tau decaying to hadrons and "lepton (ℓ)" denotes e or μ.

The Higgs boson production processes considered are (*i*) gluon gluon fusion (GGF), $gg \to H$ (+ jets); (*ii*) vector boson fusion (VBF), $q\bar{q} \to q\bar{q}H$; (*iii*) associated vector boson and Higgs boson production (VH), $q\bar{q} \to VH$, where V is a W or Z boson, and $V \to q\bar{q}$ (or $Z \to \nu\nu$ in the case of $\mu\tau$01); and (*iv*) associated Higgs boson and Z boson production (HZ), $q\bar{q} \to HZ$, with $H \to b\bar{b}$ and $Z \to \tau\tau$. The GGF, VBF, and VH processes are further subdivided according to the Higgs boson decay, $H \to \tau\tau$, $H \to WW$, or (for the $\mu\tau$01 analysis) $H \to ZZ$, and these subchannels are denoted as GGF$_{\tau\tau}$, GGF$_{WW}$ or GGF$_{ZZ}$, etc. The fractional decompositions of signal contributions expected from Monte Carlo (MC) simulations are shown in Fig. 1 for the $\mu\tau$01 and $\ell\tau$2+ selection requirements discussed below.

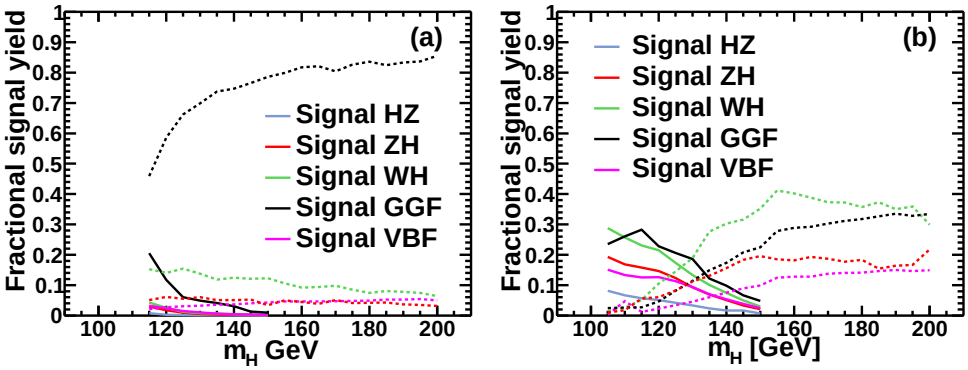

FIG. 1: (color online) Fractional yields for H signals from MC simulations as a function of M_H for (a) the $\mu\tau$01 and (b) $\ell\tau$2+ analyses. The yields for each signal process are plotted as solid lines for $H \to \tau\tau$ decays and as dashed lines for the $H \to VV$ decays.

Tau leptons can occur either through direct decays of the Higgs boson (at low mass) or indirectly from $H \to VV$ with $V \to \tau + X$ (at high mass). The leptons may arise from τ decay or (at high mass) directly from V decay. Thus the $\ell\tau$ channel is more uniformly sensitive to Higgs boson production over the full allowed mass range than are the dedicated $H \to b\bar{b}$ or $H \to WW \to \ell\bar{\ell}\nu\nu$ analyses, thus improving the combined search, particularly in the intermediate mass region around 135 GeV.

II. TRIGGER

The $\mu\tau$01 and $\mu\tau$2+ data were collected using the full inclusive suite of triggers employed in D0. The trigger efficiency for a subset of single muon triggers is measured to be about 65% using a sample of $Z \to \mu\mu$ events and is parameterized as a function of muon transverse momentum (p_T), pseudorapidity (η), azimuthal angle (ϕ), and instantaneous luminosity. Efficiency functions are computed incorporating the observed luminosity distribution in the data and are applied to the MC simulations of the background and signal processes. The ratio of events from

the inclusive trigger to those from the single muon triggers then establishes a multiplicative factor used to obtain the overall trigger efficiency. We examine the dependences of this ratio upon the p_T and η of the μ, τ and leading (highest p_T) jet. For the $\mu\tau$01 analysis, the ratio is parameterized as a function of p_T^τ. For the lower statistics $\mu\tau$2+ analysis, no significant dependences are observed, and a constant scale factor is used. The use of the inclusive trigger gives an increase in the data sample of about 40% compared to that from the single muon triggers alone.

For the $e\tau$2+ analysis, a set of triggers requiring a single electromagnetic object was used. The efficiency of these triggers is obtained from a tag and probe analysis of $Z \to ee$ events and found to be about 85% efficient for the signal processes.

III. BACKGROUND AND SIGNAL SAMPLES

The major backgrounds for the Higgs boson search are $Z+$jets, $W+$jets, $t\bar{t}$, and QCD multijet production (MJ) with misidentification of leptons or taus. Smaller backgrounds arise from boson (W, Z or γ) pair production and single top quark production. All but the MJ background are simulated using MC event generator programs and normalized to the highest order available theoretical calculations. These are referred to below as "SM" backgrounds. The MC simulations use the CTEQ6L1 parton distribution functions (PDF) [9].

The $Z+$jets and $W+$jets event samples are generated by ALPGEN [10], interfaced to PYTHIA [11] which provides initial and final state radiation and hadronization of the produced partons. The p_T^Z distribution is reweighted to agree with the D0 measurement [12]. The p_T^W is also reweighted for the $\ell\tau$2+ analyses using the same experimental input, corrected for the theoretical differences expected in next-to-next-to-leading order (NNLO) QCD [13]. For the $\ell\tau$2+ analyses, the absolute normalization for the $Z+$jets and $W+$jets cross sections are taken from Ref. [14] using the MRST2004 NNLO PDFs [15]. The same $Z+$jets normalization is used for the $\mu\tau$01 analysis but the $W+$jets normalization is derived from data as discussed below.

We simulate $t\bar{t}$ and single top quark events using the ALPGEN and COMPHEP [16] generators respectively, with PYTHIA used to simulate hadronization effects. The normalizations are based on the approximate NNLO calculations [17]. The diboson events are generated by PYTHIA.

Higgs boson production is simulated using PYTHIA, with normalizations taken from Ref. [18]. The Higgs boson decays are simulated using HDECAY [19], and the τ decays are obtained from TAUOLA [20].

All MC signal and background events are input to a GEANT3-based [21] simulation of the detector response and processed with the same reconstruction programs as used for data. Data events collected from random beam crossings are superimposed on the MC events to account for detector noise and pileup from additional $p\overline{p}$ collisions in the same or previous bunch crossings. Correction factors are applied to the simulated events to account for the trigger efficiencies and for the differences between MC and data for the lepton, tau, and jet identifications, and for the energy scale and resolution of jets.

IV. EVENT SELECTION CRITERIA

Muons selected for this analysis are required to have hits in the muon chambers before and after the toroidal magnets and to be matched to a good quality track in the tracking system with $p_T > 15$ GeV and $|\eta| < 1.6$. The muon candidate is required to be isolated in both the calorimeter and the tracking system using the calorimeter transverse energy, $E_T^{\rm iso}$, in the annular cone $0.1 < \mathcal{R} < 0.4$ around the muon, where $\mathcal{R} = \sqrt{\Delta\eta^2 + \Delta\phi^2}$, and the track transverse momentum sum, $p_T^{\rm iso} = \Sigma p_T^{\rm track}$, within in a cone $\mathcal{R} < 0.5$, excluding the p_T of candidate muon. For the $\mu\tau$01 analysis, $E_T^{\rm iso}$ and $p_T^{\rm iso}$ must be less than 15% of p_T^μ. For the $\mu\tau$2+ analysis, $E_T^{\rm iso}$ and $p_T^{\rm iso}$ must be less than 2.5 GeV. Muon candidates due to cosmic rays are rejected if the scintillation counters surrounding the detector indicate a time of arrival more than 10 ns from that expected for collision products.

Electrons are identified using a likelihood variable, $\mathcal{L}_e$, that uses as inputs the matching of the electromagnetic (EM) shower centroid to a good quality track, the fraction of energy deposited in the EM section of the calorimeter (EMF), a measure of the probability that the energy deposit pattern in the calorimeter conforms to that expected for an electron, $E_T^{\rm iso}$, and the separation along the beam axis of the electron track and the primary vertex (PV). The signal sample electrons are required to have $\mathcal{L}_e > 0.85$. Electron candidate tracks are required to have $p_T > 15$ GeV and $|\eta| < 1.1$ or $1.5 < |\eta| < 2.5$, and to impinge upon a module of the central EM calorimeter within the central 80% of its azimuthal range.

The selection of hadronically decaying tau leptons is done separately for three types based on the number of tracks within a cone $\mathcal{R} < 0.3$ and the number of EM subclusters found in the calorimeter using a nearest neighbor algorithm. Type 1, patterned on the decay $\tau_h \to \pi\nu_\tau$, requires one track and no EM subclusters. Type 2, based on $\tau_h \to \rho\nu_\tau$, requires one track and at least one EM subcluster. Type 3, motivated by the $\tau_h \to a_1\nu_\tau$ decay, requires at least two

tracks with or without EM subclusters. We reject type 3 candidates with exactly two tracks of opposite signs since their charge sign is ambiguous. The visible τ_h transverse energy, E_T^τ, is constructed from the tracking and calorimeter information. The track transverse momentum, $p_T^{\rm trk}$, is the sum of the p_T of all tracks in the τ selection cone. We require $E_T^\tau > (12.5, 12.5, 15)$ GeV, $p_T^{\rm trk} > (7, 5, 10)$ GeV, and $(p_T^{\rm trk}/E_T^\tau) > (0.65, 0.5, 0.5)$ for τ types (1, 2, 3). The leading (highest p_T) track for type 3 τs must exceed 7 GeV. A neural network, NN_τ [22], based on energy deposition patterns and isolation criteria in the calorimeter and tracking systems is constructed for each tau type to discriminate a tau from a misidentified jet. For type 2 τs, a second neural network, $\mathrm{NN}_{\tau/e}$, is constructed to differentiate taus from electrons. We require $|\eta_\tau| \leq 2$ for all tau types.

Jets are selected using an interative midpoint cone algorithm [23] with a cone size $\mathcal{R} = 0.5$. We require at least two tracks associated with the jet that point to the PV. Jet energies are corrected to the particle level for out-of-cone showering, underlying event energy deposits and pileup, and for the effects of energy carried by muons and neutrinos in the case of evidence for semileptonic decays of the jet particles. Jets are corrected for energy scale and resolution; the MC jets are corrected for energy scale and resolution, as well as for the jet identification efficiency to bring the MC responses into agreement with data. For the quark-dominated MC samples ($t\bar{t}$ and diboson), there is an additional shift in jet energy that accounts for the differences in the responses of quark jets and the dominantly gluon jets for which the jet energy scale correction was obtained. The $\mu\tau 2+$ and $e\tau 2+$ analyses require at least two jets with $|\eta_{\rm jet}| < 3.4$ and $p_T^{\rm jet} > 20$ (15) GeV for the leading (other) jet. The $\mu\tau 01$ analysis imposes these jet p_T requirements as a veto to ensure orthogonality of the analyses.

The missing transverse energy, $\not\!\!E_T$, is computed from the observed transverse energy deposits in the calorimeter and is adjusted for the appropriate energy scale corrections for all objects and for isolated muons observed in the event. For the $\ell\tau 2+$ analyses, the $\not\!\!E_T$ is apportioned to the neutrinos from the two postulated tau leptons by decomposing the $\not\!\!E_T$ vector into components associated with the observed lepton and hadronic tau [24].

For the final event selection, all three analyses require exactly one isolated lepton and a hadronic tau with opposite charges. The separations between all pairs of lepton, tau, and jets are required to be $\mathcal{R} > 0.5$. For the $\mu\tau 01$ analysis, events are required to have only one τ_h, and the smaller of the transverse masses, $m_T = \sqrt{2E_T^{\rm lepton} E_T^\nu (1 - \cos\phi(\ell, \nu))}$ (with "lepton" = τ_h or μ and $E_T^\nu = \not\!\!E_T$) must exceed 25 GeV to suppress the $Z+$ jets and MJ backgrounds, while retaining about 80% of the signal. For the $e\tau 2+$ analysis, substantial backgrounds arise from $Z +$ jets production with $Z \to ee$ where an electron is misidentified as a type 2 τ_h. To reduce these, we remove τ_h candidates in the region $1.1 < |\eta| < 1.5$ where the calorimetry has impaired electron identification. Further $Z+$ jets rejection is obtained by requiring type 2 τ_h candidates to have $\mathrm{NN}_{\tau/e} > 0.95$ to suppress electrons that resemble the track + EM cluster signature, and by rejecting type 2 τ_h candidates which point near the edge in ϕ of an EM module in the central calorimeter. In addition, type 3 τ_h candidates with EMF > 0.95 are excluded. The MJ background in the $e\tau 2+$ analysis is suppressed by requiring $\mathcal{S} > 1$ where $\mathcal{S}$ is the $\not\!\!E_T$ significance corresponding approximately to the number of standard deviations (s.d.) that the $\not\!\!E_T$ differs from zero [25].

V. BACKGROUNDS DERIVED FROM DATA

The MJ background arising from misidentification of leptons or taus by the detector reconstruction algorithms is difficult to simulate, so for each analysis, the MJ background is taken from data. The general method for all analyses is similar: we define a sample of MJ-enriched events, $\mathcal{M}$, from which residual SM backgrounds simulated by MC are subtracted, to provide the shapes of the MJ kinematic distributions. The number of MJ events in the signal sample is obtained by multiplying the MJ yield in a signal-like sample $\mathcal{N}$ by a scale factor ρ_i, obtained from the $\mathcal{M}$ sample for each of the tau types, i. The ρ_i are in all cases near one.

For the $\mu\tau 01$ channel, the sample $\mathcal{M}$ is obtained by requiring $m_T(\mu, \not\!\!E_T) < 30$ GeV and $\mathrm{NN}_\tau < 0.2$, and the ρ_i are the ratios of isolated to non-isolated lepton events in $\mathcal{M}$, and are parameterized as a function of $p_T^\tau, N_{\rm jets}$, $\not\!\!E_T$, and p_T^μ. These factors scale the MJ fraction of the sample $\mathcal{N}$, selected as for the signal sample except that the muon is required to be non-isolated, to obtain the MJ normalization in the isolated lepton signal sample. An alternate MJ-enriched sample is defined by $\mathrm{NN}_\tau < 0.2$ and $m_T(\mu, \not\!\!E_T) < 30$ GeV, in which the τ_h and μ have the same charge sign, for estimating the MJ background uncertainty.

For the $\mu\tau 2+$ analysis, the MJ sample $\mathcal{M}$ is obtained by reversing at least one of the muon isolation requirements and requiring $0.3 < \mathrm{NN}_\tau < 0.8$. The MJ fraction of this sample is 94% before the MC SM subtraction. The ρ_i factors are the ratio of opposite charge sign (OS) and same charge sign (SS) $\mu - \tau_h$ pairs in $\mathcal{M}$ and are used to scale the MJ component of the sample $\mathcal{N}$ selected as for the signal sample except that we require SS μ and τ_h. The ρ_i show no significant dependence on the kinematic variables.

For the $e\tau 2+$ analysis, $\mathcal{M}$ is obtained by requiring the electron to satisfy an orthogonal loose electron selection, $0 < \mathcal{L}_e < 0.85$, and $0.3 < \mathrm{NN}_\tau < 0.9$. The MJ fraction of this sample is 96% before the MC SM subtraction. The

ρ_i are obtained from the OS and SS $\mathcal{M}$ sample and are applied to the MJ component of the $\mathcal{N}$ sample as in the $\mu\tau 2+$ analysis. The ρ_i show no significant dependence on kinematic variables. Alternate MJ-enriched samples, in which either the τ_h or lepton selections (but not both) are reversed, are defined for estimating the MJ background uncertainties in both $\ell\tau 2+$ analyses.

For the $\mu\tau 01$ analysis, the dominant background is from $W+$jets with the muon from W decay and a jet misidentified as a tau. Both the normalization of the $W+$jets sample and the misidentification probability are difficult to model adequately, so the simulation is corrected using a data-driven method [26]. The jet produced in association with a W boson has a charge that is correlated differently with the W boson charge for quarks and gluons. Furthermore, the probability for a jet misidentified as a tau to have the same charge sign as its progenitor parton varies with NN_τ. We determine a weight for $W+$jets MC events that depends on the charge correlation between the muon and recoil parton and on the value of NN_τ.

VI. EVENT YIELDS

The numbers of data and expected background events are given in Table I for the $\mu\tau 01$, $\mu\tau 2+$, and $e\tau 2+$ analyses.

TABLE I: For each analysis channel, the number of background events expected from SM processes, MJ background, and observed data, for individual and sum of all tau types after preselection. "V+j" denotes W or Z + jets and "DB" denotes diboson processes.

τ type	$t\bar{t}$	W+j	$Z_{\ell\ell}$+j	$Z_{\tau\tau}$+j	DB	MJ	ΣBkd	Data
$\mu\tau 01$ analysis								
type 1	4.0	234	21.6	10.5	28.9	39.3	338	340
type 2	19.4	852	93.6	56.4	108	116	1245	1294
type 3	3.8	678	56.7	19.4	25.4	67.3	850	839
All	27.2	1764	172	86.3	162	223	2433	2473
$\mu\tau 2+$ analysis								
type 1	12.5	9.2	4.5	29.0	2.0	18.9	76.2	81
type 2	86.0	56.8	22.1	158.5	11.5	58.5	393.5	418
type 3	13.2	34.2	4.2	43.4	2.5	21.9	119.4	109
All	111.7	100.3	30.8	230.9	16.0	99.2	589.1	608
$e\tau 2+$ analysis								
type 1	2.2	2.4	0.3	5.6	0.8	6.0	18.0	10
type 2	14.3	21.0	14.1	30.1	1.5	25.4	106.3	98
type 3	7.0	16.2	1.8	10.5	1.4	15.4	52.4	59
All	23.6	39.6	16.2	46.1	3.6	46.8	176.1	167

VII. MULTIVARIATE ANALYSIS

The expected number of events for Higgs boson signal processes is small in comparison to the backgrounds shown in Table I. For example, the expected signal yields at $m_H = 165$ GeV are 5.2, 1.7 and 0.3 events for the $\mu\tau 01$, $\mu\tau 2+$ and $e\tau 2+$ analyses respectively. The corresponding yields at $m_H = 115$ GeV are 0.9, 1.6 and 0.4 events. We thus employ multivariate techniques that utilize both the magnitudes of the variables and the correlations among them. We choose well-modelled variables that have some capability to distinguish between signal and background processes as shown in Table II. Figure 2 shows distributions for representative variables that offer significant discrimination of signal and background for each of the channels.

The $\mu\tau 01$ analysis uses neural networks [27] (NN_H) trained for each τ_h type to discriminate between all backgrounds and all signals for $115 \leq m_H \leq 200$ GeV in 5 GeV increments. The τ_h types 1 and 3 are combined for training to improve statistics. The NN_H distributions are binned in 21 equal sized bins for $0 < \mathrm{NN}_H < 1.05$. The $\mu\tau 2+$ and $e\tau 2+$ analyses use boosted decision trees (BDT) [27] trained for all signals against the sum of all backgrounds, with all τ types combined for Higgs boson masses $105 \leq m_H \leq 200$ GeV in 5 GeV steps. The BDT output is binned in 15 bins spanning $-1 < \mathrm{BDT} < 1$ with a non-uniform binning to assure sufficiently small statistical uncertainty in the predicted backgrounds within any bin. We smooth the effects of signal MC statistics by averaging BDT distribution for m_H with the neighboring distributions at $(m_H - 5)$ GeV and $(m_H + 5)$ GeV with weights of 50%, 25%, and 25%. Figure 3 shows the NN_H distribution for the $\mu\tau 01$ analysis at $m_H = 165$ GeV and the averaged BDT distributions for the $\ell\tau 2+$ analyses at $m_H = 135$ GeV.

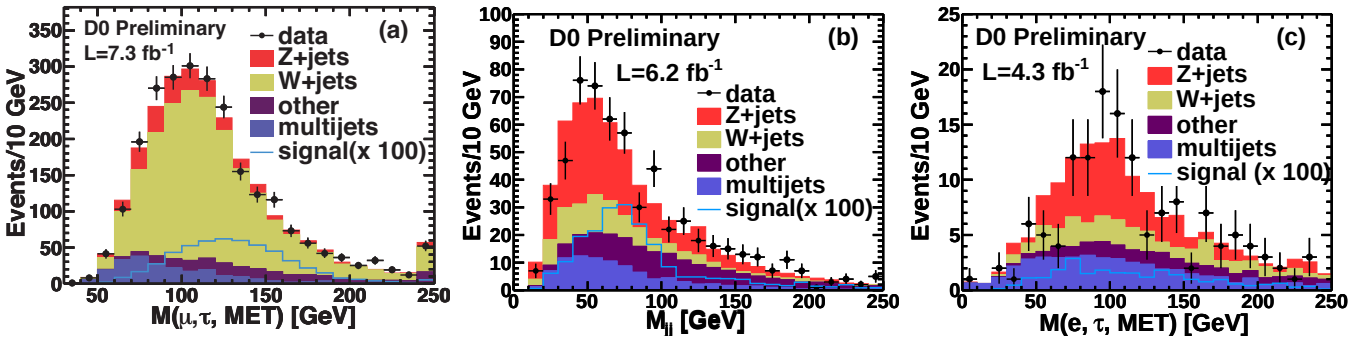

FIG. 2: (color online) Comparison of data, expected backgrounds, and total signal with the indicated scaling factors for (a) invariant mass of the μ, τ_h, $\not\!\!E_T$ system for the $\mu\tau 01$ analysis (signal shown for $m_H = 165$ GeV); (b) dijet invariant mass for the $\mu\tau 2+$ analysis (signal shown for $m_H = 150$ GeV); and (c) invariant mass of the $\tau\tau$ system for the $e\tau 2+$ analysis (signal shown for $m_H = 150$ GeV), where the $\not\!\!E_T$ contribution is apportioned to the e and τ_h as discussed in the text.

TABLE II: List of variables used in multivariate analysis for the $\mu\tau 01$ and $\ell\tau 2+$ analyses. The variable $\not\!\!H_T$ is the missing transverse energy computed from the jets in the event.

Variable	$\mu\tau 01$	$\ell\tau 2+$
Lepton p_T	x	x
Tau p_T	x	x
Leading jet p_T	x	x
$\not\!\!E_T$	x	x
μ charge $\times\eta_\mu$	x	
η_τ	x	
$\ell\tau$ invariant mass	x	x
Dijet invariant mass		x
$\mu\,\tau\,\not\!\!E_T$ invariant mass	x	
$\ell\nu$ transverse mass, m_T^ℓ		x
$\tau\nu$ transverse mass, m_T^τ		x
Minimum of m_T^ℓ and m_T^τ	x	
$\Sigma\lvert\vec{p}_T\rvert$ of all jets		x
Scalar p_T sum of ℓ, τ,$\not\!\!E_T$, jets		x
Magnitude of vector p_T sum of ℓ, τ, $\not\!\!E_T$, jets		x
Minimum $\sqrt{s}$ necessary for final objects	x	
Number of jets	x	
$\Delta\mathcal{R}$ between leading jets		x
$\Delta\eta$ between leading jets		x
Asymmetry between $\not\!\!E_T$ and $\not\!\!H_T$		x
$\Delta\phi$ between ℓ and τ	x	
$\Delta\theta$ between ℓ and τ	x	
$\Delta\phi$ between ℓ and $\not\!\!E_T$	x	
$\Delta\phi$ between τ and $\not\!\!E_T$	x	
$\Delta\phi$ between $\not\!\!E_T$ from calorimeter and tracks		x
Cosine of angle between ℓ and beam direction	x	
Minimum $\delta\phi$ between $\not\!\!E_T$ and a jet		x
Missing E_T significance, $\mathcal{S}$		x
NN_τ	x	

VIII. SYSTEMATIC UNCERTAINTIES

A large number of systematic uncertainties have been considered, typically broken down separately by analysis channel, tau type, background or signal process, or Higgs boson mass. The luminosity and trigger uncertainties are obtained from separate analyses of D0 data. The lepton, tau, and jet energy scale, resolution, and identification uncertainties are obtained from special control samples. Uncertainties in the SM background cross section normalizations and shapes are obtained using theoretical uncertainties, and the extent to which special data samples enriched in each

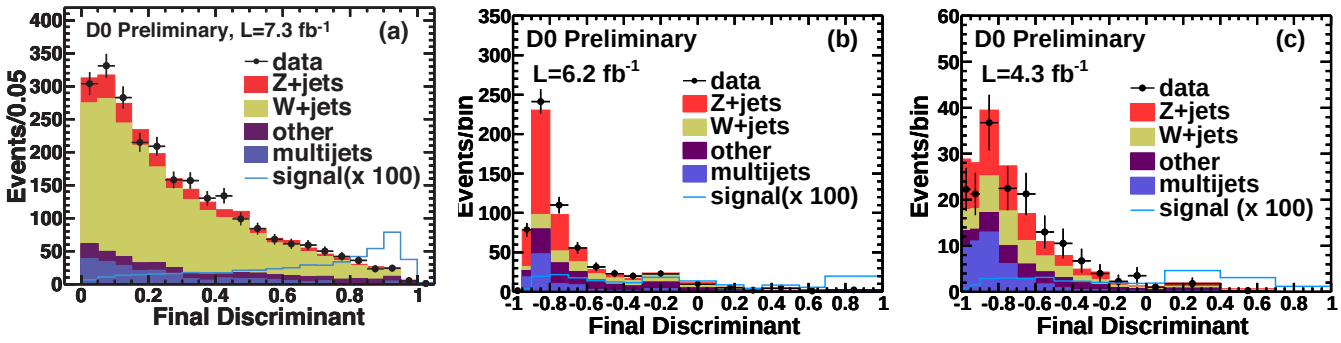

FIG. 3: (color online) (a) NN_H distribution for the $\mu\tau 01$ analysis at $m_H = 165$ GeV; (b) BDT distribution for the $\mu\tau 2+$ analysis at $m_H = 150$ GeV; and (c) BDT distribution for the $e\tau 2+$ analysis at $m_H = 150$ GeV.

background process agree with MC predictions. The MJ background uncertainties are determined by comparing the alternate MJ-enriched samples with the results obtained with the nominal choice. Signal cross section uncertainties are obtained from theoretical estimates and include the effect of PDF uncertainties. For each source, the impact on the final variable (NN_H or BDT) distribution is assessed by changing the nominal values of a parameter by ± 1 s.d. Some of the uncertainties affect only the normalization of the final variable distribution and some modify its shape.

Table III summarizes the systematic uncertainties. Many entries comprise several subcategories. For example, the jet reconstruction uncertainty includes the effects of jet identification, confirmation that the tracks within the jet arise from the PV, jet resolution and jet energy scale. Moreover, these elements of the jet reconstruction uncertainty are computed separately for different background processes and hypothesized Higgs mass values in each analysis channel.

TABLE III: The range of systematic uncertainties (in percent) for categories of their source. Each category typically summarizes several individual souces separated by analysis channel, tau type, and/or physical process. Those with "Type" indicated as "N" affect only the normalization of the final variable distribution. Those indicated as "S" affect the shape of the final variable distribution.

Source	Type	Uncertainty
Luminosity	N	6.1
Muon trigger	N	$5-9$
Electron trigger	N	2
Muon reconstruction	N	$2-3$
Electron reconstruction	N	4
Tau reconstructin	N	$4-14$
Jet reconstruction	S	$2-10$
Jet modeling	S	$0-7$
SM backgrounds	N	$5-12$
MJ background	S	$10-50$
Signal cross sections	N	$5-40$

IX. CROSS SECTION LIMITS

The upper limits on the Higgs boson cross section for each analysis are obtained from the final multivariate outputs using the modified frequentist method [28], using a negative log likelihood ratio (LLR) for the background only and signal+background hypotheses as the test statistic. For the $\mu\tau 01$ analysis, each tau type is input separately to the limit setting calculation for Higgs boson masses from 115 to 200 GeV in 5 GeV steps. The $\ell\tau 2+$ calculation uses the BDTs summed over tau type for m_H values from 105 to 200 GeV in 5 GeV steps, averaged over neighboring mass bins as described above.

The impact of systematic uncertainties on the limits is minimized by maximizing a "profile" likelihood function [29] in which these uncertainties are constrained to Gaussian priors. The value of the Higgs boson cross section is adjusted in each limit calculation until the value of CL_s reaches 0.05, corresponding to the 95% C.L., where $CL_s = CL_{s+b}/CL_b$ and CL_{s+b} (CL_b) are the probabilities for the negative LLR value observed in simulated signal+background (back-

TABLE IV: The ratio of expected and observed 95% C.L. limits on the Higgs boson cross section to the SM values for each analysis channel and the combination of all channels including that of [7].

m_H	$\mu\tau$01		$\mu\tau$2+		$e\tau$2+		Combined	
	exp	obs	exp	obs	exp	obs	exp	obs
105	–	–	17.7	18.5	33.3	58.9	12.6	17.1
110	–	–	19.3	20.8	34.3	55.7	12.9	17.7
115	84.2	106.4	20.3	26.3	37.5	55.1	14.3	21.8
120	42.9	31.1	19.2	23.3	40.5	59.4	13.7	15.6
125	34.2	37.5	17.3	19.5	42.3	64.9	12.8	15.7
130	25.2	32.4	15.9	20.6	44.2	72.5	11.5	17.9
135	20.3	20.3	17.5	15.2	47.2	82.5	11.3	11.8
140	16.7	20.0	18.7	13.2	44.7	68.1	11.1	10.1
145	13.8	13.3	18.3	12.9	43.5	54.2	11.3	9.8
150	11.9	12.8	17.9	13.6	45.4	54.1	10.8	9.5
155	9.8	12.9	18.2	13.2	42.3	57.5	9.2	9.0
160	8.2	7.6	19.1	11.1	33.9	74.9	8.4	7.6
165	8.1	7.8	21.7	11.2	32.8	69.8	7.7	6.8
170	8.5	9.4	21.3	12.7	35.2	64.5	8.5	7.4
175	9.5	8.6	22.7	11.4	40.7	73.7	9.6	8.0
180	12.2	13.5	22.1	14.6	45.5	84.6	11.4	11.0
185	13.5	12.1	25.7	19.8	53.7	90.8	12.2	9.7
190	16.5	17.2	29.5	19.1	58.8	101.8	14.6	12.3
195	18.5	18.7	30.1	20.9	67.3	110.4	16.1	15.3
200	19.2	31.5	28.9	26.9	69.3	114.4	19.8	29.9

ground) pseudo-experiments to be less than that observed in our data. The limits obtained are summarized in Table IV.

We combine the information from the three channels by recomputing the LLR and limits for the three analyses together, now also including the limits from the previous 1 fb^{-1} $\mu\tau$2+ analysis [7]. In this calculation, the systematic uncertainties across the different analyses are appropriately correlated (e.g. the Z + jets normalization for all channels is the same). The fully combined LLR distributions and the 95% C.L. limits as a function of m_H are shown in Figs. 4 and 5. The combined limits are also shown in Table IV.

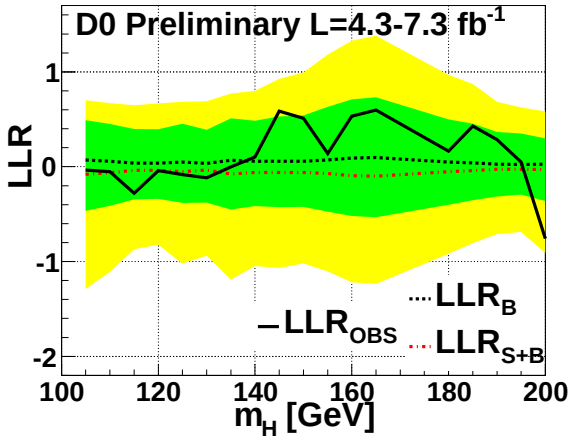

FIG. 4: (color online) The LLR distribution as a function of m_H showing the expected LLR distributions for the background only and signal+background hypotheses, and the observed LLR, for the combination of all channels. The green (yellow) bands show the ±1 s.d. (±2 s.d.) bands around the expected background only LLR values.

In summary we have searched for the SM Higgs boson in final states involving an electron or muon and a hadronically decaying tau. We set 95% C.L. limits on the Higgs boson production cross section which are 21.8 and 6.8 times those

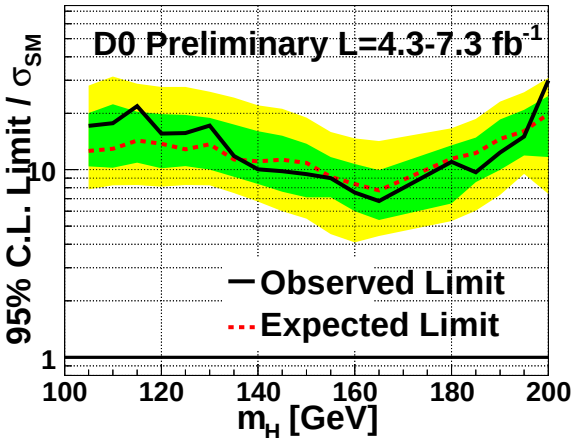

FIG. 5: (color online) The ratio of observed and expected Higgs boson cross section limits to those expected in the SM, for the combination of all channels. The green (yellow) bands show the ±1 s.d. (±2 s.d.) bands around the expected ratios.

expected in the SM for Higgs boson masses of 115 and 165 GeV.

We thank the staffs at Fermilab and collaborating institutions, and acknowledge support from the DOE and NSF (USA); CEA and CNRS/IN2P3 (France); MON, Rosatom and RFBR (Russia); CNPq, FAPERJ, FAPESP and FUNDUNESP (Brazil); DAE and DST (India); Colciencias (Colombia); CONACyT (Mexico); NRF (Korea); FOM (The Netherlands); STFC and the Royal Society (United Kingdom); MSMT and GACR (Czech Republic); BMBF and DFG (Germany); SFI (Ireland); The Swedish Research Council (Sweden); and CAS and CNSF (China).

[1] R. Barate *et al.* (LEP Working Group for Higgs boson searches), Phys. Lett. B **565**, 61 (2003).
[2] The CDF and D0 Colaborations, arXiv:hep-ex/1107.5518 (2011).
[3] The ATLAS Collaboration, arXiv:hep-ex/1202.1408 (2012); the CMS Collaboration, arXiv:hep-ex/1202.1488 (2012).
[4] M. Baak *et al.* (GFitter collaboration), arXiv:hep-ph/1107.0975 (2011).
[5] D0 Collaboration, D0 Note 6229-CONF (2011).
[6] CDF Collaboration, CDF Note 10609-CONF (2011).
[7] V.M. Abazov *et al.* (D0 Collaboration), Phys. Rev. Lett. **102**, 251801 (2009).
[8] S. Abachi *et al.* (D0 Collaboration), Nucl. Instrum. Methods Phys. Res. A **338**, 185 (1994); V.M. Abazov *et al.* (D0 Collaboration), Nucl. Instrum. Methods Phys. Res. A **565**, 463 (2006); V.M. Abazov *et al.*, Nucl. Instrum. Methods Phys. Res. A **552**, 372 (2005).
[9] J. Pumplin *et al.*, J. High Energy Phys. **0207**, 012 (2002).
[10] M.L. Mangano *et al.*, J. High Energy Phys. **0307**, 001 (2003).
[11] T. Sjöstrand *et al.*, arXiv:hep-ph/030815 (2003).
[12] V.M. Abazov *et al.* (D0 Collaboration), Phys. Rev. Lett. **100**, 102002 (2008).
[13] K. Melnikov and F. Petriello, Phys. Rev. D **74**, 114017 (2006).
[14] R. Hamburg, W.L. van Neerven, and W.B. Kilgore, Nucl. Phys. **B359**, 343 (1991); **B644**, 403 (2002).
[15] A.D. Martin, R.G. Roberts, W.J. Stirling, and W.B. Kilgore, Phys. Lett. B **604**, 61 (2004).
[16] E. Boos *et al.*, Phys. Atom. Nucl. **69**, 1317 (2006); E. Boos *et al.* (CompHEP Collaboration), Nucl. Instrum. Methods Phys. Res. A **534**, 250 (2004).
[17] N. Kidonakis, Phys. Rev. D **74**, 114012 (2006); S. Moch and P. Uwer, Phys. Rev. D **78**, 34003 (2008).
[18] J. Baglio and A. Djouadi, arXiv:hep-ph/1003.4266v2 (2010).
[19] A. Djouadi, J. Kalinowski, and M. Spira, Comp. Phys. Commun. **108**, 56 (1998).
[20] S. Jadach *et al.*, Comp. Phys. Commun. **76**, 361 (1993).
[21] R. Brun and F. Carminati, CERN Program Library Long Writeup W5013, 1993 (unpublished).
[22] V.M. Abazov *et al.*(D0 Collaboration), Phys. Lett. B **670**, 292 (2009).

[23] G. Blazey *et al.* in *Proceedings of the Workshop: QCD and Weak Boson Physics in Run II*, edited by U. Baur, R.K. Ellis and D. Zeppenfeld, Fermilab-Pub-00/297 (2000).
[24] T. Sjöstrand *et al.* Comp. Phys. Commun. **135**, 238 (2001).
[25] A. Schwartzman, FERMILAB-THESIS-2004-21 (2004).
[26] R. Madar, FERMILAB-THESIS-2011-39 (2011).
[27] A. Hoecker *et al.*, `arXiv:physics/0703039v5` (2007).
[28] A. Read, J. Phys. G: Nucl. Part. Phys. **28**, 2693 (2002); T. Junk, Nucl. Instrum. Methods Phys. Res. A **434**, 435 (1999).
[29] W. Fisher, FERMILAB-TM-2386-E (2007).